JOURNAL OF GUIDANCE, CONTROL, AND DYNAMICS
Vol. 34, No. 3, May–June 2011

Targeting Ballistic Lunar Capture Trajectories Using Periodic Orbits

Paul Ricord Griesemer* and Cesar Ocampo†
University of Texas at Austin, Austin, Texas 78712
and
D. S. Cooley‡
NASA Goddard Space Flight Center, Greenbelt, Maryland 20771

DOI: 10.2514/1.46843

A particular periodic orbit in the Earth–sun circular restricted three-body problem is shown to have the characteristics needed for a ballistic lunar capture transfer. An injection from a circular parking orbit into the periodic orbit serves as an initial guess for a nonlinear targeting algorithm. By targeting appropriate parameters incrementally in increasingly complicated force models and using precise derivatives calculated from the state transition matrix, a reliable algorithm is produced. Ballistic lunar capture trajectories in restricted four-body systems are produced in a systematic way.

Nomenclature

$\mathbf{a}$	=	acceleration vector of spacecraft in a coordinate system centered on Earth–moon barycenter
c	=	Jacobi constant in circular restricted three-body problem
$\boldsymbol{c}$	=	constraint vector in targeting and optimization algorithms
$F(t)$	=	state propagation matrix
f_m	=	true anomaly in moon-centered coordinate frame
J	=	performance index in optimization algorithm
KE_m	=	Keplerian energy with respect to moon
$\mathbf{r}$	=	position vector of spacecraft in a coordinate system centered on Earth–moon barycenter
$\mathbf{r}_{L2}$	=	position vector of L_2
$r_{L_2/m}$	=	distance of L_2 from moon
$\mathbf{r}_m$	=	position vector of moon in a coordinate system centered on the Earth–moon barycenter
r_p	=	perigee radius
$\mathbf{r}_s$	=	position vector of sun in a coordinate system centered on the Earth–moon barycenter
r_1	=	distance of spacecraft to primary in the circular restricted three-body problem
r_2	=	distance of spacecraft to secondary in the circular restricted three-body problem
$\mathbf{v}$	=	velocity vector of spacecraft in a coordinate system centered on the Earth–moon barycenter
$\mathbf{X}$	=	state vector
$\mathbf{x}_p$	=	vector of free parameters in targeting and optimization algorithms
$\Phi(t_f, t_0)$	=	state transition matrix
α	=	parking orbit inclination in ecliptic frame
β	=	parking orbit longitude of ascending node in ecliptic plane
γ	=	parking orbit true anomaly in ecliptic plane
ΔV	=	magnitude of transfer trajectory insertion burn
λ	=	eigenvalue of monodromy matrix
μ	=	mass ratio in circular restricted three-body problem
μ_e	=	gravitational parameter of Earth
μ_m	=	gravitational parameter of moon
μ_s	=	gravitational parameter of sun

Introduction

A BALLISTIC lunar capture trajectory is characterized by a spacecraft transitioning from a hyperbolic lunar orbit into a captured lunar orbit without the need of a maneuver at the time of transition. The trajectories were initially developed using the concept of the weak stability boundary (WSB), a chaotic region of phase space that exists around masses in multibody problems. Trajectories of this type were first developed by Belbruno in 1987 [1]. Belbruno and Miller [2] were able to use the WSB in combination with the sun's gravitational influence to successfully place a satellite in lunar orbit in 1991. Presented here is a new method of targeting lunar transfers of this type that can be inserted into from low Earth orbit (LEO). A particular family of periodic orbits in the sun–Earth circular restricted three-body problem (CRTBP) is used to generate a reference trajectory, which is used as an initial guess in a nonlinear targeting routine.

Several methods of designing ballistic lunar capture transfers have been documented [3–11]. Belbruno and Carrico [3] have presented a two-dimensional, user-in-the-loop forward targeting algorithm for transfers that approach the moon along an orbit that has an apogee that is much greater than the distance from the Earth to the moon. Yamakawa et al. [4] used a shooting method to produce similar transfers in the planar restricted four-body problem (RFBP). Additional algorithms exist that use the invariant manifolds associated with libration point orbits in the sun–Earth and Earth–moon CRTBPs. For example, Koon et al. [5] targeted ballistic lunar capture trajectories by finding intersections of these invariant manifolds. Similarly, Yamato and Spencer [6] approximated the invariant manifolds in a perturbed CRTBP, yielding transit orbits. Parker and Lo [7] have categorized families of ballistic lunar capture trajectories found from invariant manifolds with the intention of allowing a mission planner to choose appropriate trajectories for specific missions. Alternatively, Biesbroek et al. [8] have used genetic algorithms to successfully find WSB trajectories. Finally, Yagasaki [9] has created a nonlinear boundary value problem that obtains a solution by beginning with an elliptic arc in the two-body problem (mass parameters of the sun and moon equal to zero) and iterating the

Received 23 August 2009; revision received 5 March 2010; accepted for publication 12 March 2010.

*Graduate Student, Department of Aerospace Engineering and Engineering Mechanics, 1 University Station C0600.
†Associate Professor, Department of Aerospace Engineering and Engineering Mechanics, 1 University Station C0600.
‡Aerospace Engineer, Navigation and Mission Design Branch, Mail Stop 595.0.

solution with increasing mass parameters of the sun and moon until the real-world solution is obtained.

Other ballistic lunar capture transfer targeting methods exist that do not rely on solar gravitational effects. The trajectories that these transfers target depart an Earth orbit and approach the moon from the direction of the interior Earth–moon Lagrange point. Conley [10] was the first to study this type of low energy transfer via transit orbits. Bollt and Meiss [11] developed a targeting scheme in the Earth–moon planar CRTBP that relies on recurrence of chaotic trajectories. Macau and Grebogi [12] used a similar method to target transfers to the moon through chaotic spaces in the restricted three-body problem (RTBP) through elimination of recurrent orbits; however, improved transfer times over Bollt and Meiss [11] were achieved at the expense of a second maneuver and higher fuel costs. Both of these methods rely on very large parking orbits around the Earth to achieve a low energy impulsive transfer without the need of a solar perturbation. Mengali and Quarta [13] also disregard the solar gravitational influence when they compare their planar three-body bi-impulsive method to WSB transfers.

The targeting of ballistic lunar capture trajectories poses problems because of the chaotic nature of the trajectory and the complexity of the four-body dynamics that are required to produce them. The WSB is by definition a chaotic region in phase space where small changes in the state of a spacecraft will lead to large variations in its trajectory. In addition, ballistic lunar captures that rely on a single impulsive maneuver to transfer from the Earth to the moon require the gravitational dynamics of the sun, Earth, and moon. The four-body dynamical system makes systematic convergence to ballistic lunar capture trajectories problematic. These problems cannot be avoided, but strategies for successful convergence can be formulated by taking into account the complex nature of the system.

In this paper, ballistic lunar capture transfers are approximated in a simpler dynamical system for the purpose of creating initial guesses accurate enough to converge to solutions in a numerical targeting scheme. A similar approximation was made by Ivashkin [14] in comparing them to bielliptic transfers in a central body gravity field. In this comparison, the solar perturbation of the Earth-centered two-body problem provides the intermediate ΔV that increases the perigee distance of the orbit. From Lidov [15], an estimation of the effect of this perturbation on the perigee distance can be made. Although the comparison of a bielliptic transfer with a ballistic lunar capture trajectory has been shown by these authors to be geometrically appropriate, the dynamics of the ballistic lunar capture trajectory can be better demonstrated in a three-body model.

The solar effect on perigee can be seen in a family of periodic orbits in the sun–Earth CRTBP. These periodic orbits explicitly exhibit the influence of the sun on the low energy transfers. A targeting algorithm is described that uses a particular member of a family, documented by Markellos [16] as family $f16$, as a generating trajectory for an Earth–moon transfer in the RFBP. The algorithm overcomes the stated difficulties in numerically seeking ballistic lunar capture trajectories by using an incremental approach from an appropriate initial guess and derivatives based on the state transition matrix. The given parameters for the algorithm are the initial transfer date and the properties of a low Earth parking orbit. Using the generating trajectory as an initial guess, the complexities of the four-body problem are added to the targeting algorithm incrementally until the final trajectory is converged upon.

Circular Restricted Three-Body Problem

The reference trajectory for the targeting algorithm is developed in the sun–Earth CRTBP [17]. This problem describes the motion of an infinitesimally small mass through space. Its motion is perturbed by the gravitational attraction of two other bodies: a primary point mass and a secondary point mass that is less massive than or equally massive to the mass of the primary. The primary body in the system is the sun, with a normalized mass equal to $1-\mu$, and the secondary body is an object, with the combined mass of the Earth and the moon, located at the Earth–moon barycenter, with a normalized mass equal to μ, shown in Eq. (1):

$$\mu = \frac{\mu_e + \mu_m}{\mu_e + \mu_m + \mu_s} \tag{1}$$

A coordinate system is established with an origin collocated with the secondary body. It has a rotation rate that fixes the x axis to the line connecting the primary mass and the secondary mass. The z axis is in the direction of the angular momentum of the system, and the y axis completes the right-handed frame. The units of the coordinate system are scaled such that the distance between the primary and secondary masses is unitary and the rotation rate of the coordinate system is 1 rad per time unit.

The motion of the spacecraft in the CRTBP defined previously is governed by Eq. (2):

$$\ddot{\mathbf{r}} = -\frac{1-\mu}{r_1^3}\begin{pmatrix} r_x+1 \\ r_y \\ r_x \end{pmatrix} - \frac{\mu}{r_2^3}\begin{pmatrix} r_x \\ r_y \\ r_z \end{pmatrix} + 2\begin{pmatrix} \dot{r}_y \\ -\dot{r}_x \\ 0 \end{pmatrix} + \begin{pmatrix} r_x+1-\mu \\ r_y \\ 0 \end{pmatrix} \tag{2}$$

where the vector $\mathbf{r}$ is the position vector in the CRTBP coordinates described previously, r_1 is the distance from the spacecraft to the primary, and r_2 is the distance from the spacecraft to the secondary.

An integral of motion known in the system, the Jacobi integral, is shown in Eq. (3). The mass parameter μ for the system, with the sun as the primary and the Earth and moon combined into a single secondary body, is $3.040364489 \times 10^{-6}$:

$$c = (r_x+1-\mu)^2 + r_y^2 + 2\frac{1-\mu}{r_1} + 2\frac{\mu}{r_2} - (\dot{r}_x^2 + \dot{r}_y^2 + \dot{r}_z^2) \tag{3}$$

Family $f16$ Periodic Orbits

In the three-body problem, it is useful to look at periodic orbits as a tool for understanding the dynamics. According to the conjecture by Poincaré [18], the population of periodic orbits in the CRTBP is dense, ensuring that for every orbit there is a periodic orbit an infinitesimally small distance away in phase space. Here, periodic orbits around the secondary body (in this system, the Earth–moon combined mass) are used to demonstrate perigee-increasing effects of the sun on the spacecraft. Markellos [16] provided a survey of families of periodic orbits in the CRTBP. If Markellos's family f is extended such that the trajectories pass nearer to the secondary body, periodic orbits can be generated that have the desired effects on the perigee radii of the orbit. Figure 1 shows an example of such an orbit from family $f16$ in Markellos's catalog. The trajectory is shown in a

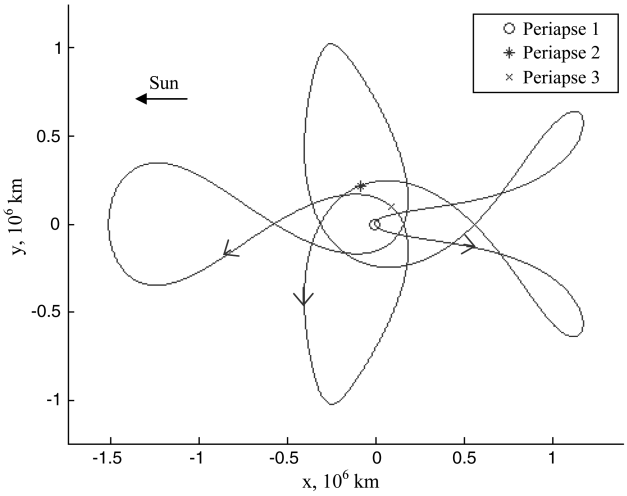

Fig. 1 Periodic orbit from Markellos's family $f16$ in rotating coordinates centered on the Earth–moon combined mass.

Table 1 Periapse distances in orbit $f16$

Periapse	Radial distance, km
1	7,200
2	230,434
3	132,580

rotating reference frame centered on the Earth–moon barycenter and with the sun located on the negative x axis. It demonstrates the effect of the sun's gravity on the periapse of an orbit about the secondary mass in the CRTBP. The solar perturbation of the two-body elliptical orbit increases the periapse radius between the first and second flybys, labeled in Fig. 1 as periapse 1 and periapse 2, respectively. The magnitude of the third periapse is also greatly increased when compared with the first periapse. The periodic orbit has five periapses in total, with periapses 4 and 5 symmetric reflections of periapses 3 and 2, respectively. Table 1 compares the periapse radii of the three unique flybys. The orbit has the following defining properties: initial $\times$ value $= 4.81290 \times 10^{-5}$, and the Jacobi constant is equal to 3.000852115.

A similar periodic orbit can be found that is nearly a reflection of the orbit in Fig. 1 about the y axis of the rotating coordinate system centered at the Earth–moon combined mass. The orbit shown in Fig. 2, labeled here $f'16$, displays the same periapse-raising characteristics as its counterpart in family $f16$.

An important characteristic of the orbits defined by families $f16$ and $f'16$ is that members of the family can be defined by a single parameter. For example, given a value for the nearest periapse location that falls in the range of existence for the family, a unique member of the family can be defined. The orbits can therefore be scaled so that the nearest periapse may coincide with a predefined LEO. Similarly, the Jacobi constant of the orbit can be used as a defining parameter. Given a value of the Jacobi energy, a member of each family can be found.

From Miele [19] and Szebehely, [17] an orbit in the CRTBP that makes two perpendicular crossings of the x axis is necessarily periodic due to the symmetries in the equations of motion. Both of the orbits detailed cross the x axis perpendicularly at their nearest and farthest points from the secondary body. These periodic orbits are five periodic orbits of the second kind, indicating that four nonperpendicular x-axis crossings exist in between perpendicular crossings. In total, the orbit crosses the x axis 10 times.

Periodic orbits of this type can be easily found using differential correction [20]. The trajectory begins at the nearest periapse, located on the x axis with a velocity perpendicular to the x axis. The trajectory is propagated from that point with an initial velocity that yields an appropriate Jacobi constant until the x axis is crossed five times. The initial velocity is then adjusted through an iterative process to yield a trajectory that has zero velocity in the x direction at the fifth crossing of the x axis. The converged initial conditions are then propagated forward for twice the amount of time, and the periodic orbit is established.

Figure 3 shows the families $f16$ and $f'16$ parameterized by the location of the nearest periapse and the corresponding Jacobi constant. Both families are shown to terminate at the secondary body, $x = 0$. As the nearest periapse moves away from the secondary, the family continues until an encounter is made with a zero velocity surface. A selection of orbits from family $f'16$ is shown in Fig. 4, including the orbits that have the nearest and farthest close approaches to the secondary body. In the case of the orbit with the farthest close approach, with a nearest periapse radius $r_p = 2.687608 \times 10^{-4}$, it is seen that this orbit has a near interaction with a zero velocity surface, as evidenced by the near reversal of direction at the first apoapse after the nearest periapse.

The families can be further characterized by their stability properties. From Broucke [21], a sufficient condition for stability of a periodic orbit in the restricted problem is having the eigenvalues of the monodromy matrix, or the state transition matrix calculated for one full period, lie on the unit circle on the complex plane. The computation of the state transition matrix is discussed next in the context of forming partial derivatives for the correction procedure. Figures 5–7 show the magnitude of the six eigenvalues of the monodromy matrices for the families. From these figures, family $f'16$ can be clearly understood to be unstable, as every orbit has eigenvalues that do not lie on the unit circle. Family $f16$ has a region of stability where all eigenvalues have unit magnitude. These stable orbits are well outside the region that would include LEOs. The periodic orbits used in this work are unstable orbits.

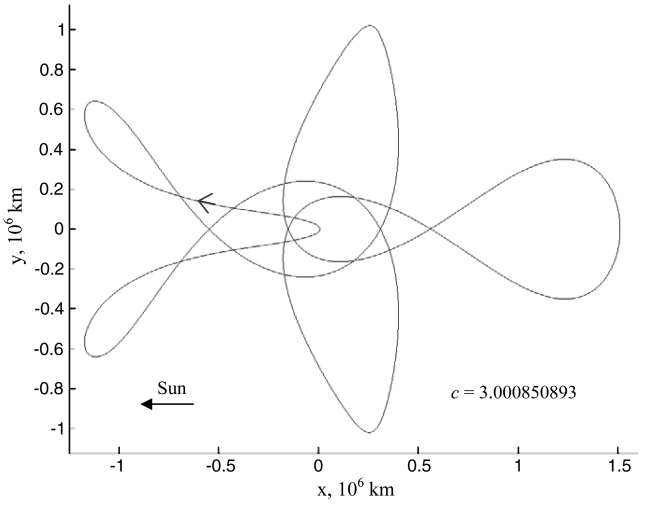

Fig. 2 Periodic orbit $f'16$ in rotating coordinates centered on the Earth–moon combined mass.

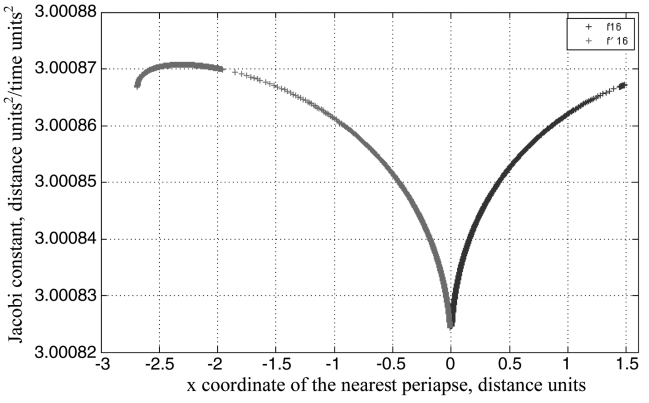

Fig. 3 Parameterization of families $f16$ and $f'16$.

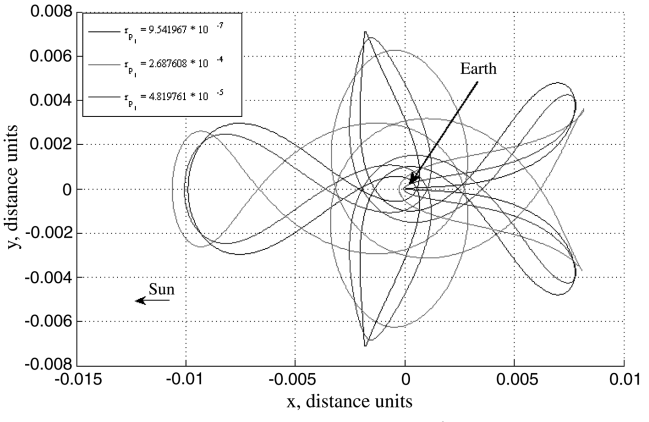

Fig. 4 Selection of orbits from the $f'16$ family.

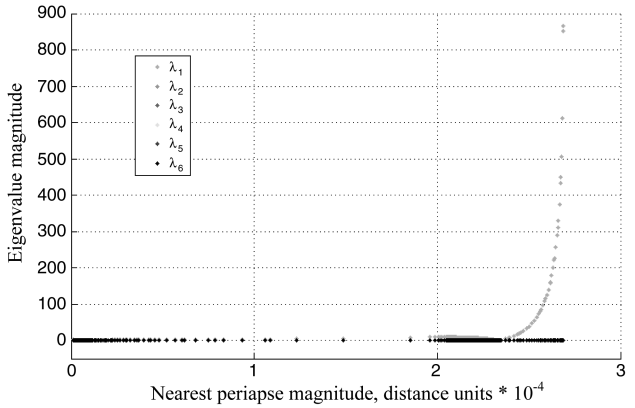

Fig. 5 Eigenvalue magnitudes of the monodromy matrices of family $f'16$.

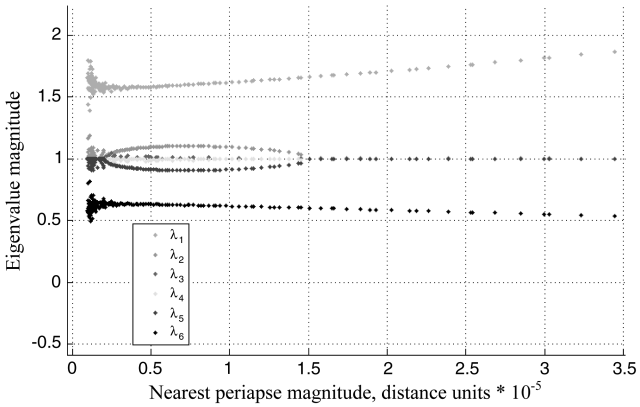

Fig. 6 Zoom of eigenvalue magnitudes of the monodromy matrices of family $f'16$.

As detailed in Table 1, this periodic orbit can be used to increase the periapse of a spacecraft's orbit without a maneuver. The reference trajectory for the ballistic lunar capture targeting algorithm will begin with an insertion into a family member of the shown periodic orbits at the nearest periapse, labeled periapse 1 in Fig. 1, and end at one of the other periapses. The periodic orbit will be selected from family $f16$ or $f'16$ to coincide at the nearest periapse with the radius of the parking orbit of the satellite. Any of the periapses along the periodic orbit that have had their radii increased could then be used to target ballistic lunar capture trajectories. The work in this paper, however, covers only examples for achieving capture at the first and second periapses. If the first periapse is targeted, the transfer trajectory from

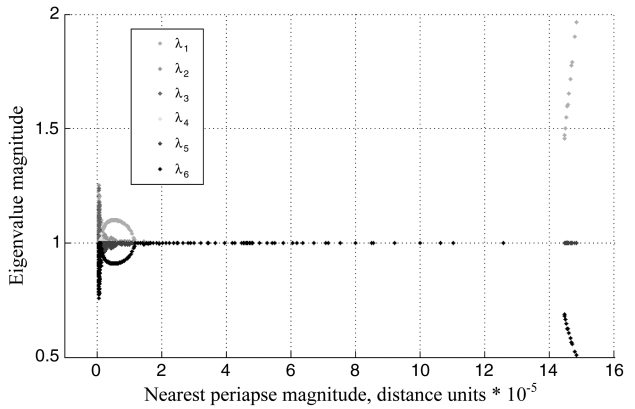

Fig. 7 Eigenvalue magnitudes of the monodromy matrices of family $f16$.

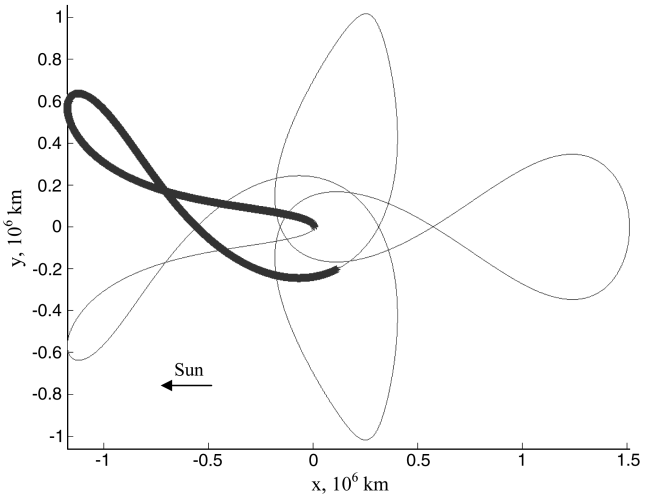

Fig. 8 Reference trajectory for a $f'16p1$ transfer in rotating coordinates centered on the Earth–moon combined mass.

LEO to lunar orbit will have a period of approximately 100 days, and the reference trajectory is shown in bold in Fig. 8. The reference trajectory shown in Fig. 8 is labeled $f'16p1$ to denote that it is from the generating family $f'16$ and targets a capture at the first increased periapse. In the case of targeting the second periapse, the period becomes approximately 180 days, and the reference trajectory, shown in Fig. 9, is labeled $f'16p2$ due to its generating family and its target for capture at the second periapse. It should be noted that none of the periapse radii in the periodic orbits are equal to, or even closely approximate, the lunar distance from the Earth. These trajectories make suitable reference orbits because they display the dynamics necessary for the periapse to increase.

Converged solutions that resulted from the reference trajectories of the two different periods are shown in Figs. 10 and 11. The solutions are not geometrically identical to the reference trajectories. The periodic orbits simply provide initial guesses that reliably allow convergence to ballistic lunar capture transfers. The selection of the appropriate periodic orbit for the reference trajectory from the generating families $f16$ and $f'16$ will be discussed in a following section.

Targeting Algorithm

An algorithm to incrementally step from the reference trajectory presented previously to a ballistic lunar capture trajectory in a

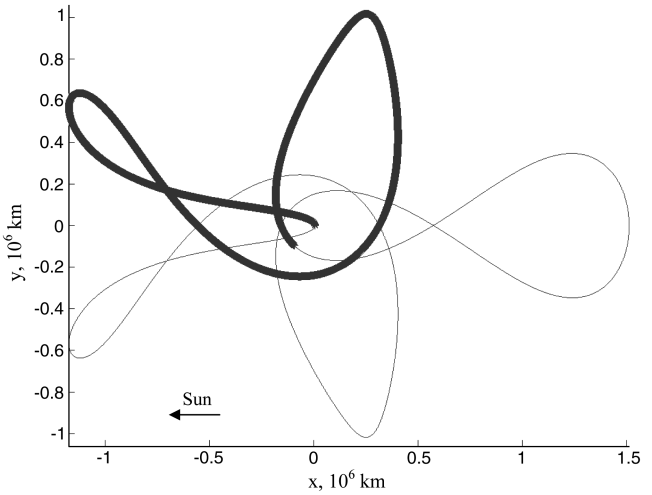

Fig. 9 Reference trajectory for a $f'16p2$ transfer in rotating coordinates centered on the Earth–moon combined mass.

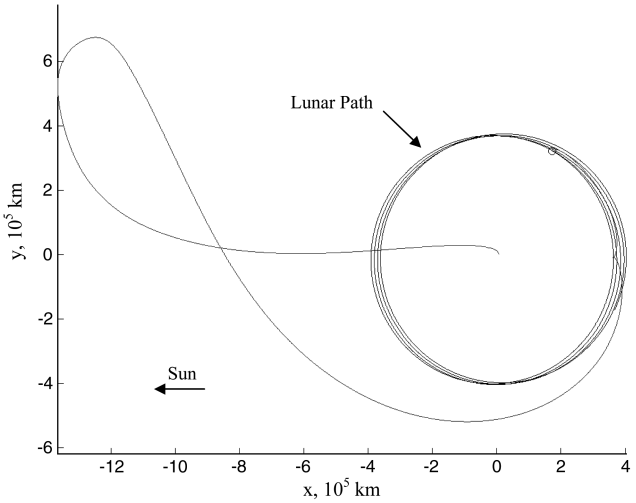

Fig. 10 A $f'16p1$ transfer in Earth-centered sun–Earth rotating coordinates.

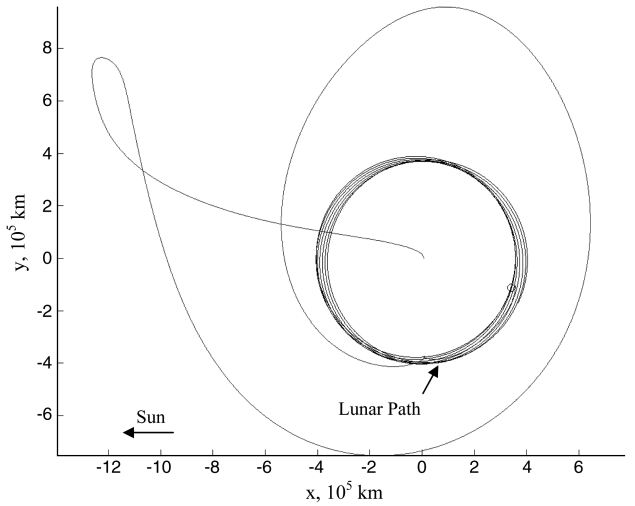

Fig. 11 A $f'16p2$ transfer in Earth-centered sun–Earth rotating coordinates.

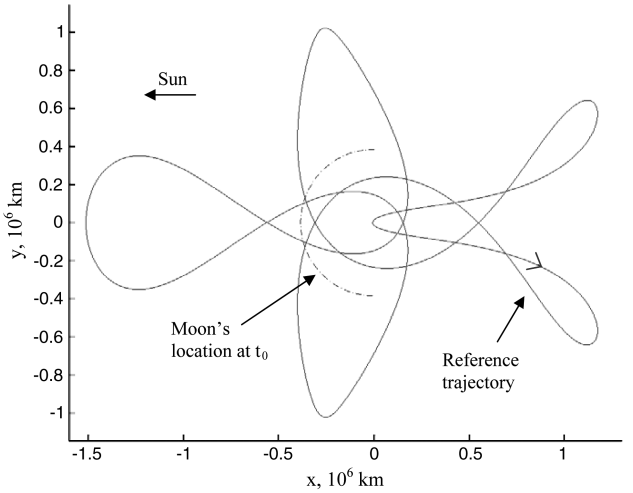

Fig. 12 Lunar position for generating family $f16$ selection in Earth-centered rotating coordinates.

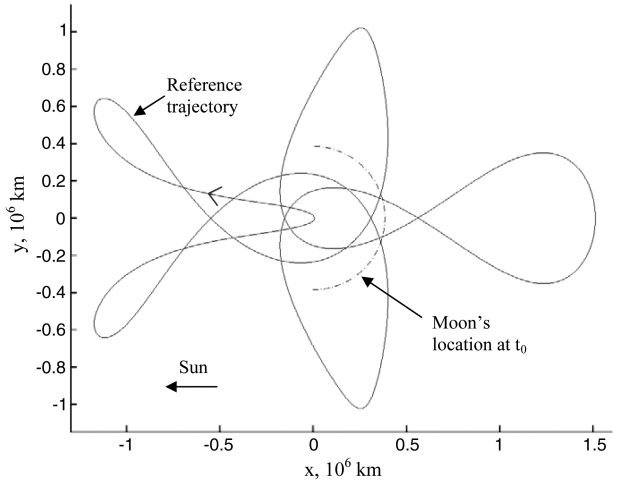

Fig. 13 Lunar position for generating family $f'16$ selection in Earth-centered rotating coordinates.

realistic ephemeris model is presented here. An incremental approach is used to increase the stability and reliability of the algorithm. In each step, elements of the realistic system are added, increasing the complexity of the dynamics from the CRTBP used in the formulation of the reference trajectory and transitioning to the ephemeris model. In this algorithm, the radius of the initial parking orbit and the desired initial time of the transfer are given parameters. The converged solution provides the orientation of the parking orbit and the ΔV that will result in a captured lunar orbit.

Transfer Orientation

The initial task of the targeting algorithm is to select the proper family of generating orbits from the two generating families, $f16$ and $f'16$. One of the factors of the reliability of the targeting algorithm is the effect of the moon's gravity on the outbound leg of the ballistic lunar capture trajectory. Depending on the orientation of the moon with respect to the trajectory, the lunar perturbation can vary greatly. To increase the stability of the algorithm, a transfer orientation with the farthest distance from the moon is chosen in order to mitigate the effect of the moon on this leg of the transfer. Trajectories that employ a lunar flyby on the outbound segment can have advantages in cost savings, but they are not presented here due to their adverse affects on the numerical routine's convergence.

Insertion into either of the two possible transfers can be achieved with a ΔV in the direction of the velocity vector of the spacecraft in a prograde low Earth parking orbit. The selection of the appropriate class of trajectory to target on a given launch date is made based on the location of the moon in the sun–Earth rotating coordinate frame at the time of the transfer. If the moon is located in the quadrants of the coordinate system farthest from the sun, then the $f'16$ generating family should be used, maximizing the distance between the moon and the spacecraft. If the moon is located in a quadrant nearest to the sun, then the generating family $f16$ is appropriate. Figures 12 and 13 illustrate the selection of the reference trajectory. In the example ballistic lunar capture trajectory described next, the family $f'16$ is appropriate for the given epoch.

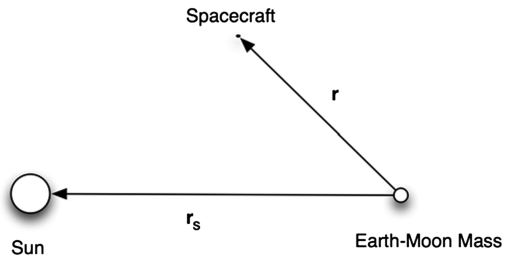

Fig. 14 RTBP.

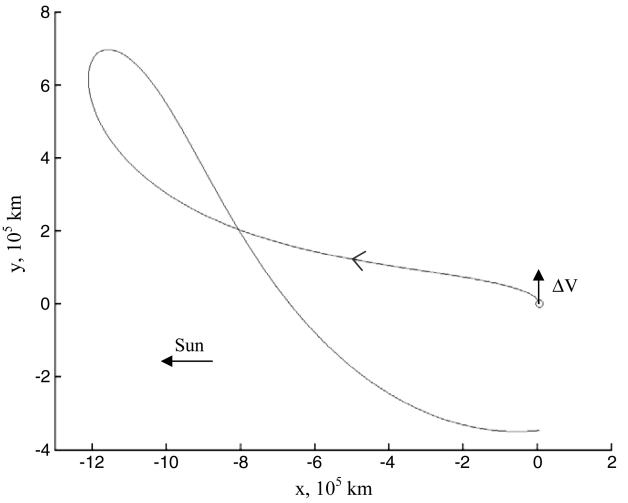

Fig. 15 Crossing of the *y* axis in rotating coordinates centered on the Earth–moon combined mass.

Estimation of Transfer Time

The first step in the targeting algorithm is to estimate the transfer duration. The initial time is provided among the given parameters. An estimation of the final time is made so that it coincides with one of the moon's crossings of the *y*-*z* plane in the Earth-centered Earth–sun rotating coordinates. There are two crossings of the *y*-*z* plane each month: one in the positive-*y* direction and one in the negative-*y* direction. The appropriate crossing is selected to correspond to the orientation of the reference trajectory. For example, in the $f'16$ trajectories, the appropriate final time is the time of the moon's passage from the third quadrant to the fourth quadrant of the rotating coordinate system. To allow for the appropriate phasing, the final time is selected to be that of the crossing that occurs nearest to the time of the periapse that is being used as the initial guess for the transfer. Regardless of the initial time, the final time will be chosen based on the orientation of the moon in rotating coordinates as described. By following this procedure, the initial time is arbitrary, but a spacecraft will arrive at the moon at one of two possible times during each month.

ΔV Targeting in Restricted Three-Body Problem

With an estimation of the transfer time, the first targeting step can be performed. This first step adjusts $\Delta V0$ in the planar problem to account for the difference in the flight time of the nominal transfer in the CRTBP and the estimated flight time found in the previous step, thereby phasing the transfer to arrive at the moon. If the initial time were not a fixed parameter, then this step would be unnecessary.

Following the method developed by Pu and Edelbaum [22], an approximate $\Delta V0$ for the four-body problem is calculated in a three-body problem by adding the mass of the moon to the mass of the Earth and scaling the orbit radius. The combined mass is located at the Earth–moon barycenter. The radius of the initial parking orbit is

Table 2 First iteration step

	t_0	Parking orbit radius, km	ΔV, km/s	Δt, days
Initial	2453611	7200	3.08568	117.31800
Solution	2453611	7200	3.04875	117.31800

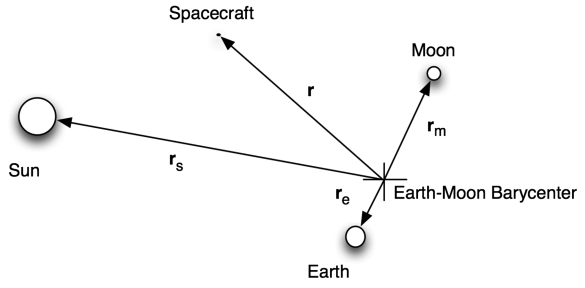

Fig. 16 RFBP.

then adjusted to produce the same circular velocity around the combined mass object as the original parking orbit around the Earth, as shown in Eq. (4):

$$r_2 = r_1 \frac{\mu_e + \mu_m}{\mu_e} \tag{4}$$

This three-body problem allows a good approximation of the ΔV required to insert the spacecraft into the transfer. An initial guess of the ΔV is determined by taking the difference between the spacecraft's circular velocity and its velocity at the closest flyby on the reference trajectory. For this step, the orientation of the parking orbit is fixed in the orbital plane of the Earth–moon barycenter around the sun, and only the magnitude of the initial burn is varied. The ΔV is assumed to be oriented in the direction of the spacecraft's velocity vector.

In the numerical propagation of the trajectory, the sun and the Earth–moon combined masses are both treated as point masses. Their locations are determined from the Jet Propulsion Laboratory (JPL) DE405 [23] ephemeris. The trajectory of the spacecraft is propagated in a nonrotating coordinate frame centered on the Earth–moon combined mass, shown in Fig. 14, and the motion in the RTBP is governed by Eq. (5):

$$\ddot{\mathbf{r}} = -\frac{\mu_e + \mu_m}{r^3}\mathbf{r} - \frac{\mu_s}{|r - r_s|^3}(\mathbf{r} - \mathbf{r}_s) - \frac{\mu_s}{r_s^3}\mathbf{r}_s \tag{5}$$

A differential correction algorithm is used in this targeting step [20]. Let x_p be the vector of parameters that are varied to satisfy the targeting constraints. The vector c contains the constraints that must be driven to zero in the numerical routine. The differential correction algorithm estimates the derivative of x_p with respect to c in order to find the correction of x_p to make c approach the zero vector.

For this targeting step, there is only one free parameter, $x_p = \Delta V$. The target is the spacecraft's crossing of the *y*-*z* plane of the Earth–moon barycenter centered sun–(Earth–moon) rotating coordinate system at t_f, $c = r_x$. The transversal of the *y*-*z* plane will occur in the bottom half of the *x*-*y* plane if observed from above, resulting in a trajectory similar to the trajectory shown in Fig. 15.

As can be seen in Fig. 15, the solar influence on the orbit has raised the orbit's periapse at the second flyby. Table 2 details the parameters of the first iteration step for the sample trajectory shown in Fig. 15.

Parking Orbit Orientation Selection in Restricted Three-Body Problem

With the preceding result obtained, the approximate ΔV has been established for the ballistic lunar capture trajectory. Continuing with Pu and Edelbaum's [22] approximation of the four-body problem, the approximate orientation of the initial parking orbit should be obtained before attempting to propagate the trajectory in the more complicated four-body dynamical system.

Table 3 Second iteration step results

	t_0, Julian date	α, rad	β, rad	γ, rad	ΔV, km/s	Δt, days
Initial	2453611	0.00000	0.40907	2.70878	3.04875	117.31800
Solution	2453611	0.30940	0.11059	2.92604	3.04843	117.31800

Table 4 Restricted four-body targeting step

	t_0, Julian date	α, rad	β, rad	γ, rad	ΔV, km/s	Δt, days
Initial	2453611	0.30940	0.11059	2.92604	3.04843	117.31800
Solution	2453611	0.30232	0.15788	2.99543	3.04845	117.31800

Table 5 Minimization of Keplerian energy

	t_0, Julian date	α, rad	β, rad	γ, rad	ΔV, km/s	Δt, days	KE, km^2/s^2
Initial	2453611	0.30232	0.15788	2.99543	3.04845	117.31800	−0.05379
Solution	2453611	0.30940	0.11059	2.92604	3.04837	126.59640	−0.10116

Let α, β, and γ be the orientation angles for the parking orbit. These angles define the position of a spacecraft in a circular orbit of a given radius, and they are analogous to the inclination, the longitude of the ascending node, and the true anomaly, respectively. They differ from orbital elements only in that they are defined relative to the x-y plane of the solar system as opposed to the equatorial plane of the Earth. In the targeting algorithm, the orientation angles represent the orientation of the spacecraft at the time of the transfer insertion burn. The transformation from a set of orientation angles to Cartesian coordinates is shown in Eq. (6):

$$\mathbf{r} = r\begin{pmatrix} \cos\beta\cos\alpha - \sin\beta\sin\alpha\cos\gamma \\ \cos\beta\sin\alpha + \sin\beta\cos\alpha\cos\gamma \\ \sin\beta\sin\gamma \end{pmatrix}$$
$$\mathbf{v} = \sqrt{\frac{\mu}{r}}\begin{pmatrix} -\cos\alpha\sin\beta - \cos\beta\sin\alpha\cos\gamma \\ -\sin\alpha\sin\beta + \cos\beta\cos\alpha\cos\gamma \\ \sin\gamma\cos\beta \end{pmatrix} \tag{6}$$

Using the definition of the correction scheme described previously, the four free variables in Eq. (7) are iterated from their values that were used in the last targeting step to target a point on the y axis in the sun–(Earth–moon) rotating coordinate system. The target should be at a distance from the combined Earth–moon mass equal to the distance from the Earth to the collinear Lagrange point of the Earth–moon three-body system exterior to the moon, $\mathbf{c} = \mathbf{r} - \mathbf{r}_{L2}$. In this iteration step, four parameters are used to target a three-dimensional point:

$$\mathbf{x}_p = (\,\Delta V \quad \alpha \quad \beta \quad \gamma\,)^T \tag{7}$$

The result of the previous iterations should provide approximate solutions for the orientation of the spacecraft at the time of the transfer insertion burn as well as the magnitude of the burn, which is oriented along the direction of the velocity vector of the spacecraft. The approximation is shown to be accurate to converge to a solution in the complex dynamics of the sun–Earth–moon four-body problem. Table 3 details the results of the second iteration step, continuing the targeting of the example trajectory in Fig. 15.

Targeting in Restricted Four-Body Problem

At this stage of the algorithm, the masses of the moon and the Earth are decoupled, and a more realistic system is used. The numerical stability of any targeting algorithm continues to be an issue, and the ballistic lunar capture trajectory is targeted in two steps.

The four free parameters used in the previous targeting step are used again in the four-body system. Equations of motion governing the four-body problem are now used. The three gravitational bodies are treated as point masses located at positions determined from the JPL DE405 ephemeris. The coordinate system in which the trajectory is propagated is a nonrotating frame centered at the Earth–moon barycenter, shown in Fig. 16. Equation (8) shows the RFBP equations of motion with an indirect term to account for the acceleration of the origin of the coordinate system:

$$\ddot{\mathbf{r}} = -\frac{\mu_e}{|r - r_e|^3}(\mathbf{r} - \mathbf{r}_e) - \frac{\mu_m}{|r - r_m|^3}(\mathbf{r} - \mathbf{r}_m) - \frac{\mu_s}{|r - r_s|^3}(\mathbf{r} - \mathbf{r}_s) - \frac{\mu_s}{r_s^3}\mathbf{r}_s \tag{8}$$

The target in this iteration is the spacecraft's radial distance from the moon. The iteration is considered successful if the final radial distance from the moon is less than the distance from the moon to $L2$ of the Earth–moon three-body system. In this case, the constraint is an inequality constraint, $r_{sc/m} \leq r_{L_2/m}$. The parameter vector $\mathbf{x}_p$ is the same as the previous targeting step [Eq. (7)]. Table 4 shows the details of the four-body targeting step.

Energy Minimization in Restricted Four-Body Problem

The final step of the targeting algorithm is a constrained minimization of the spacecraft's Keplerian energy with respect to the moon. In this minimization step, let $J = \mathrm{KE}_m$ be the scalar performance index to be minimized by a sequential quadratic programming algorithm.[§] The final time of the transfer is included with the initial time and the orientation angles of the parking orbit as free variables, shown in Eq. (9):

$$\mathbf{x}_p = (\,\Delta V \quad \alpha \quad \beta \quad \gamma \quad t_f\,)^T \tag{9}$$

The constraint in this step forces the trajectory to end at a perilune. This constraint, $c = f_m$, aids in convergence to trajectories that do not crash into the moon and complete an orbit of the moon without escaping. If desired, an additional inequality constraint may be added to ensure the perilune distance is sufficient to avoid collision with the lunar surface.

After a few iterations, the minimization results in a negative Keplerian energy. If a particular orbit around the moon is desired, constraints can be added to the minimization problem that will yield the desired orbit, possibly with another small burn. The results of the targeting algorithm are shown in Table 5, and the capture trajectory is displayed in Fig. 10. It is noteworthy that the trajectory already possesses negative energy with respect to the moon before this iteration step; however, the minimization of energy is necessary to produce a trajectory that remains captured by the moon for a significant period of time. Figure 17 shows the transfer resulting in a captured orbit for at least one revolution.

Success Criteria

A successful targeting algorithm will systematically produce captured trajectories. In a multibody system, however, the definition of capture is problematic. In the two-body problem, a negative Keplerian energy is sufficient for ensuring the spacecraft will not escape the system. Similarly, in the RTBP, a Jacobi energy value that produces zero velocity surfaces that constrain the motion of the spacecraft to one of the primary bodies is an identifier of a captured spacecraft. In the four-body problem used in the targeting algorithm, there are no constant energylike quantities that bind the motion of the

[§]Data available at http://hsl.rl.ac.uk/archive/hslarchive.html [retrieved 29 January 2011].

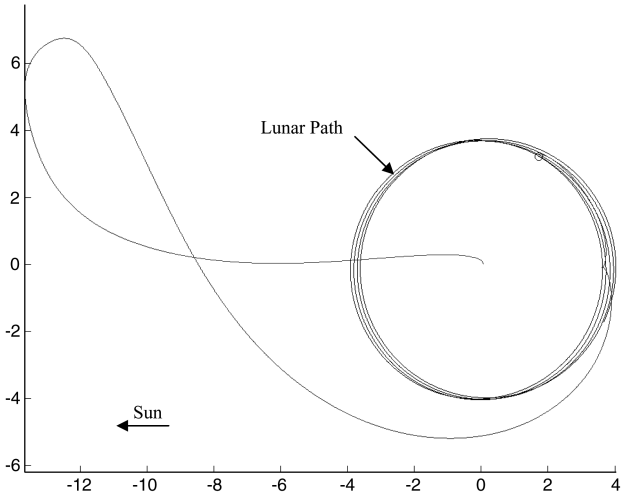

Fig. 17 Ballistic lunar capture transfer in the ephemeris model.

spacecraft. This problem has been previously dealt with in several ways. Belbruno, in defining the WSB, defines a weakly captured trajectory as a trajectory that completes an orbit of a body, returning to the vertical plane from which it began, with negative Keplerian energy [1]. In finding WSB transfers using manifolds in the RTBP, Koon et al. define a successful transfer as one that transits through the planar libration orbit into the system of the secondary body [5].

The following three metrics for evaluating the capture of a spacecraft into lunar orbit are proposed to evaluate the success of the targeting algorithm. At the conclusion of the final step of the algorithm, the trajectory is at a perilune. Although termination at perilune is not required in the algorithm to have negative Keplerian energy with respect to the moon, a successfully captured trajectory should have negative energy at this point. The first metric used to evaluate the algorithm is whether a solution is found that has negative Keplerian energy with respect to the moon at this point. Furthermore, a second, more stringent metric is used that demands a binding of the motion of the spacecraft to the moon. Under the second metric, the algorithm is considered to be successful if there is a second perilune with negative Keplerian energy as the trajectory is propagated forward, ensuring an orbit of the moon. Finally, a third metric is used to ensure against collision. Under this metric, the algorithm is deemed to be successful if it meets the previous two requirements, and the perilune radii are greater than the moon's radius.

Algorithm Validation

Low energy transfers are shown to be found in a systematic way when periodic orbits in the CRTBP are used to initialize the algorithm. To validate the robustness of the technique, a computer program was designed to implement the algorithm described previously with the goal of computing a low energy lunar transfer on a user supplied date. Transfers of class $f16p1$ and $f'16p1$ were computed in an automated way. The program was then supplied with a randomly generated date and time between 1 January 2010 and 1 January 2012, and a low energy lunar transfer was calculated for that date. The program was fed 1000 randomly generated dates and times. The results of the run are shown in Table 6.

Table 6 Algorithm results

Parameter	Value
Number of runs	1000
Criteria 1 (negative energy)	100%
Criteria 2 (orbit)	96.50%
Criteria 3 (orbit, no collision)	91.10%

Table 7 Gravitational parameter values

Gravitational parameter	Value, km^3/s^2
μ_s	1.32715×10^{11}
μ_e	3.986004×10^5
μ_m	4.9029×10^3

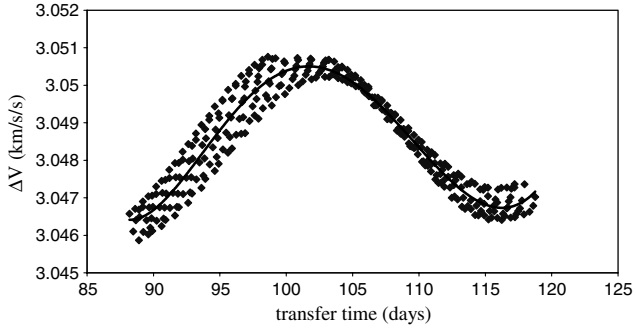

Fig. 18 Ballistic lunar capture transfer ΔV versus transfer time.

The results of this routine provide some insight on the costs associated with ballistic lunar capture transfer trajectories. Figure 18 shows the relationship between ΔV and the transfer time for the computed transfers. A trend is clear in which a maximum cost is required for transfers between 100 and 105 days. It is also noted that the difference between the maximum and minimum costs is only approximately 5 m/s. Thus, for an arbitrary orbit insertion time, the solution generated at that time is likely within a few meters per second of the cheapest solution. It should be noted that this algorithm explicitly avoids lunar flybys on the outbound leg; therefore, even the most efficient transfers may be improved upon by targeting a lunar flyby.

Software Models

The numerical trajectory propagation was performed assuming the gravitational bodies act as point masses. Unless otherwise noted, the locations of the point masses were determined using the DE405 ephemeris. The equations of motion as described in the preceding sections are integrated using DLSODA [24]. For both the numerical nonlinear equation solving and minimization functions, VF13AD was used. In all simulations, the values of the gravitational parameters used are listed in Table 7.

Conclusions

An efficient, robust method of targeting ballistic lunar capture trajectories is presented. The use of a periodic trajectory from family $f16$ in the CRTBP with the sun as the primary mass and an Earth–moon combined body as the secondary mass demonstrates the solar effect in raising the periapse of the spacecraft's orbit to approximately lunar radius. This reference trajectory serves as an excellent initial guess in the targeting algorithm that produces ballistic lunar capture trajectories on arbitrary launch dates and times. The numerical difficulties of targeting chaotic trajectories in the sun–Earth–moon four-body problems are effectively handled by the use of gradients obtained through the numerical propagation of the state transition matrix. It is shown that ballistic lunar capture transfer trajectories can be computed from random trajectory insertion dates, and the cost of the transfer varies only slightly with the transfer insertion date.

This algorithm simplifies the computation of ballistic lunar capture transfers. Implementations that contain this algorithm could potentially automate the computation of low energy transfers to the moon, opening up their analysis to a larger community of mission planners. Furthermore, the efficiency of this computation should enable a mission planner to easily analyze a wide range of transfers, enabling optimization of the low energy transfer and an understanding of what the limits in fuel savings, and the parameters that affect them, may be via ballistic lunar capture transfer.

Appendix: Sensitivity Equations

The preceding algorithm relies on a differential correction algorithm and a sequential quadratic programming routine. Zimmer and Ocampo [25] have demonstrated the benefits in accuracy from using state transition matrix derivatives as opposed to finite difference methods. Perturbations in the free variables are related to perturbations in the constraint values using the chain rule. The targeting algorithm relies on partial derivatives relating both the final state and the final value of the Keplerian energy to the five control parameters listed in Eq. (9). For the orientation angle α, the partial derivatives are written in the form

$$\frac{\partial \mathrm{KE}_f}{\partial \alpha} = \frac{\partial \mathrm{KE}_f}{\partial \mathbf{X}_f}\frac{\partial \mathbf{X}_f}{\partial \mathbf{X}_0}\frac{\partial \mathbf{X}_i}{\partial \alpha} \tag{A1}$$

and

$$\frac{\partial \mathbf{X}_f}{\partial \alpha} = \frac{\partial \mathbf{X}_f}{\partial \mathbf{X}_0}\frac{\partial \mathbf{X}_i}{\partial \alpha} \tag{A2}$$

where

$$\frac{\partial \mathbf{X}_f}{\partial \mathbf{X}_0} = \Phi(t_f, t_0) \tag{A3}$$

$$\frac{\partial \mathrm{KE}_f}{\partial \mathbf{X}_f} = \begin{bmatrix} \frac{\mu_m}{r_m^3}(x - x_m) & \frac{\mu_m}{r_m^3}(y - y_m) & \frac{\mu_m}{r_m^3}(z - z_m) & v_x - v_{mx} & v_y - v_{my} & v_z - v_{mz} \end{bmatrix} \tag{A4}$$

and

$$\frac{\partial \mathbf{X}_i}{\partial \alpha} = \begin{pmatrix} r(-\sin\alpha\cos\beta - \cos\alpha\sin\beta\cos\gamma) \\ r(\cos\alpha\cos\beta - \sin\alpha\sin\beta\cos\gamma) \\ 0 \\ v(\sin\alpha\sin\beta - \cos\alpha\cos\beta\cos\gamma) \\ v(-\cos\alpha\sin\beta - \sin\alpha\cos\beta\cos\gamma) \\ 0 \end{pmatrix} \tag{A5}$$

Similarly, the partial derivatives relating to the orientation angle β are written as

$$\frac{\partial \mathrm{KE}_f}{\partial \beta} = \frac{\partial \mathrm{KE}_f}{\partial \mathbf{X}_f}\frac{\partial \mathbf{X}_f}{\partial \mathbf{X}_0}\frac{\partial \mathbf{X}_i}{\partial \beta} \tag{A6}$$

and

$$\frac{\partial \mathbf{X}_f}{\partial \beta} = \frac{\partial \mathbf{X}_f}{\partial \mathbf{X}_0}\frac{\partial \mathbf{X}_i}{\partial \beta} \tag{A7}$$

where the partial derivative of the Keplerian energy with respect to the final state is given in Eq. (A13), the partial derivative of the final state with respect to the initial state is given as the state transition matrix, and

$$\frac{\partial \mathbf{X}_i}{\partial \beta} = \begin{pmatrix} r(-\cos\alpha\sin\beta - \sin\alpha\cos\beta\cos\gamma) \\ r(-\sin\alpha\sin\beta + \cos\alpha\cos\beta\cos\gamma) \\ r\cos\beta\sin\gamma \\ -v(\cos\alpha\cos\beta - \sin\alpha\sin\beta\cos\gamma) \\ -v(\sin\alpha\cos\beta + \cos\alpha\sin\beta\cos\gamma) \\ -v\sin\alpha\sin\gamma \end{pmatrix} \tag{A8}$$

The partial derivatives relating to the orientation angle γ are

$$\frac{\partial \mathrm{KE}_f}{\partial \gamma} = \frac{\partial \mathrm{KE}_f}{\partial \mathbf{X}_f}\frac{\partial \mathbf{X}_f}{\partial \mathbf{X}_0}\frac{\partial \mathbf{X}_i}{\partial \gamma} \tag{A9}$$

and

$$\frac{\partial \mathbf{X}_f}{\partial \gamma} = \frac{\partial \mathbf{X}_f}{\partial \mathbf{X}_0}\frac{\partial \mathbf{X}_i}{\partial \gamma} \tag{A10}$$

where the partial derivative of the Keplerian energy with respect to the final state is given in Eq. (A13), the partial derivative of the final state with respect to the initial state is given as the state transition matrix, and

$$\frac{\partial \mathbf{X}_i}{\partial \gamma} = \begin{pmatrix} r\sin\alpha\sin\beta\sin\gamma \\ -r\cos\alpha\sin\beta\sin\gamma \\ r\sin\beta\cos\gamma \\ v(\sin\alpha\cos\beta\sin\gamma) \\ -v(\cos\alpha\cos\beta\sin\gamma) \\ v\cos\beta\cos\gamma \end{pmatrix} \tag{A11}$$

The initial maneuver produces the partial derivatives

$$\frac{\partial \mathrm{KE}_f}{\partial \Delta V} = \frac{\partial \mathrm{KE}_f}{\partial \mathbf{X}_f}\frac{\partial \mathbf{X}_f}{\partial \mathbf{X}_0}\frac{\partial \mathbf{X}_i}{\partial \Delta V} \tag{A12}$$

and

$$\frac{\partial \mathbf{X}_f}{\partial \Delta V} = \frac{\partial \mathbf{X}_f}{\partial \mathbf{X}_0}\frac{\partial \mathbf{X}_i}{\partial \Delta V} \tag{A13}$$

where the partial derivative of the Keplerian energy with respect to the final state is given in Eq. (A13), the partial derivative of the final state with respect to the initial state is given as the state transition matrix, and

$$\frac{\partial \mathbf{X}_i}{\partial \Delta V} = \begin{pmatrix} \mathbf{0}_{3\times 1} \\ \Delta V(-\cos\alpha\sin\beta - \sin\alpha\cos\beta\cos\gamma) \\ \Delta V(-\sin\alpha\sin\beta + \cos\alpha\cos\beta\cos\gamma) \\ \Delta V\cos\beta\sin\gamma \end{pmatrix} \tag{A14}$$

Finally, the partial derivative of the final state with respect to the final time does not include the state transition matrix:

$$\frac{\partial \mathrm{KE}_f}{\partial t_f} = \frac{\partial \mathrm{KE}_f}{\partial \mathbf{X}_f}\frac{\partial \mathbf{X}_f}{\partial t_f} \tag{A15}$$

where

$$\frac{\partial \mathbf{X}_f}{\partial t_f} = \begin{pmatrix} \mathbf{v}_f \\ \mathbf{a}_f \end{pmatrix} \tag{A16}$$

and $\mathbf{a}_f$ is defined in Eq. (8) for the four-body problem and in Eq. (5) for the three-body problem.

References

[1] Belbruno, E. A., "Lunar Capture Orbits, A Method of Constructing Earth–Moon Trajectories and the Lunar GAS Mission," AIAA Paper 1987-1054, May 1987.

[2] Belbruno, E. A., and Miller, J. K., "Sun-Perturbed Earth-to-Moon Transfers with Ballistic Capture," *Journal of Guidance, Control, and Dynamics*, Vol. 16, No. 4, 1993, pp. 770–775. doi:10.2514/3.21079

[3] Belbruno, E. A., and Carrico, J. P., "Calculation of Calculation of WSB Ballistic Lunar Transfer Trajectories Ballistic Lunar Transfer Trajectories," AIAA Paper 2000-4142, August 2000.

[4] Yamakawa, H., Kawaguchi, J., Ishii, N., and Matsuo, H., "A Numerical Study of Gravitational Capture Orbit in the Earth–Moon System," American Astronautical Soc. Paper 1992-0186, Springfield, VA, Feb. 1992.

[5] Koon, W. S., Lo, M. W., Marsden, J. E., and Ross, S. D., "Low Energy Transfer to the Moon," *Celestial Mechanics and Dynamical Astronomy*,

Vol. 81, No. 1–2, 2001, pp. 63–73.
doi:10.1023/A:1013359120468

[6] Yamato, H., and Spencer, D. B., "Transit-Orbit Search for Planar Restricted Three-Body Problems with Perturbations," *Journal of Guidance, Control, and Dynamics*, Vol. 27, No. 6, 2004, pp. 1035–1045.
doi:10.2514/1.4524

[7] Parker, J. S., and Lo, M. W., "Families of Low-Energy Lunar Halo Orbit Transfers," American Astronautical Soc. Paper 2006-0132, Springfield, VA, Feb. 2006.

[8] Biesbroek, R. G. J., Ockels, W. J., and Janin, G., "Optimisation of WSB Orbits from GTO to the Moon Using Genetic Algorithms," International Astronautical Federation Paper 99-A.6.10, Paris, Oct. 1999.

[9] Yagasaki, K., "Sun-Perturbed Earth-to-Moon Transfers with Low Energy and Moderate Flight Time," *Celestial Mechanics and Dynamical Astronomy*, Vol. 90, Nos. 3–4, 2004, pp. 197–212.
doi:10.1007/s10569-004-0406-8

[10] Conley, C., "Low Energy Transit Orbits in the Restricted Three Body Problem," *SIAM Journal on Applied Mathematics*, Vol. 16, No. 4, 1968, pp. 732–746.
doi:10.1137/0116060

[11] Bollt, E. M., and Meiss, J. D., "Targeting Chaotic Orbits to the Moon Through Recurrence," *Physics Letters A*, Vol. 204, No. 5–6, 1995, pp. 373–378.
doi:10.1016/0375-9601(95)00502-T

[12] Macau, E. E. N., and Grebogi, C., "Control of Chaos and its Relevancy to Spacecraft Steering," *Philosophical Transactions of the Royal Society A*, Vol. 364, No. 1846, 2006, pp. 2463–2481.
doi:10.1098/rsta.2006.1835

[13] Mengali, G., and Quarta, A. A., "Optimization of Biimpulsive Trajectories in the Earth–Moon Restricted Three-Body System," *Journal of Guidance, Control, and Dynamics*, Vol. 28, No. 2, 2005, pp. 209–216.
doi:10.2514/1.7702

[14] Ivashkin, V. V., "On the Moon-to-Earth Trajectories with Gravitational Escape from the Moon Attraction," *Doklady Physics*, Vol. 49, No. 9, 2004, pp. 539–542.
doi:10.1134/1.1810582

[15] Lidov, M. L., "The Evolution of Orbits of Artificial Satellites of Planets Under the Action of Gravitational Perturbations of External Bodies," *Planetary and Space Science*, Vol. 9, No. 10, 1962, pp. 719–759.
doi:10.1016/0032-0633(62)90129-0

[16] Markellos, V. V., "Numerical Investigation of the Planar Restricted Three-Body Problem II: Regions of Stability for Retrograde Satellites of Jupiter as Determined by Periodic Orbits of the Second Generation," *Celestial Mechanics and Dynamical Astronomy*, Vol. 10, No. 1, 1974, pp. 87–134.
doi:10.1007/BF01261880

[17] Szebehely, V., *Theory of Orbits*, Academic Press, New York, 1967, pp. 7–40.

[18] Poincaré, H., *Les Méthodes Nouvelles de la Mécanique Céleste*, Vols. 1–3, Gauthier-Villars, Paris, 1892; also Dover, New York, 1957, pp. 79–156.

[19] Miele, A., "Theorem of Image Trajectories in the Earth–Moon Space," *Astronautica Acta*, Vol. 6, No. 225, 1960, pp. 225–232.

[20] Battin, R. H., *An Introduction to the Mathematics and Methods of Astrodynamics*, AIAA, Reston, VA, 1999, pp. 456–461.

[21] Broucke, R., "Stability of Periodic Orbits in the Elliptic Restricted Three-Body Problem," *AIAA Journal*, Vol. 7, No. 6, 1969, pp. 1003–1009.
doi:10.2514/3.5267

[22] Pu, C. L., and Edelbaum, T. N., "Four-Body Trajectory Optimization," *AIAA Journal*, Vol. 13, No. 3, 1975, pp. 333–336.
doi:10.2514/3.49700

[23] Standish, E. M., "JPL Planetary and Lunar Ephemerides, DE405/LE405," Jet Propulsion Laboratory Interoffice Memo. 312.F-98-048, Pasadena, CA, Aug. 1998.

[24] Hindmarsh, A. C., "Large Ordinary Differential Equation Systems and Software," *IEEE Control Systems Magazine*, Vol. 2, No. 4, 1982, pp. 24–30.
doi:10.1109/MCS.1982.1103756

[25] Zimmer, S., and Ocampo, C., "Analytical Gradients for Gravity Assist Trajectories Using Constant Specific Impulse Engines," *Journal of Guidance, Control, and Dynamics*, Vol. 28, No. 4, 2005, pp. 753–760.
doi:10.2514/1.9917